Council on Tall Buildings and Urban Habitat Korea

International Journal of
High-Rise Buildings
www.ctbuh-korea.org/ijhrb/index.php

International Journal of High-Rise Buildings
December 2024, Vol 13, No 4, 333-348
https://doi.org/10.21022/IJHRB.2024.13.4.333

Structural Design of China Merchants Bank Headquarters Tower: Part 2 – Performance-Based Seismic Design

Yueqi Hou[1], Xuan Xu[2], Mingchen Liu[1], Sen Wang[2], Xiaonian Duan[1†], and Lian Wei[2]

[1]*Structural Engineering Group, Foster + Partners, London, United Kingdom*
[2]*Shenzhen Lipeng Engineering Research & Structural Design, Shenzhen, China*

Abstract This paper presents the performance-based seismic design procedure and nonlinear seismic analysis methods and key results, as well as seismic performance evaluation of China Merchants Bank Headquarters Tower to Service-Level Earthquake, Design Earthquake and Maximum Considered Earthquake shaking. Work presented herein represents a recent example and the state-of-the-practice of performance-based seismic design and analysis, expert panel review, and independent 3rd party validation of nonlinear response history analysis results of code-exceeding supertall buildings exceeding 300 m in height. The benefits of the present Chinese practice and energy dissipating outrigger trusses using Buckling-Restrained Braces as web diagonal members are highlighted. An opportunity is identified for simplifying detailing of the boundary elements in shear walls in tall and supertall buildings located in high wind but moderate seismic regions.

Keywords Performance-Based Seismic Design, Nonlinear Response History Analysis

†Corresponding author:
Xiaonian Duan
E-mail:
xduan@fosterandpartners.com

1. Introduction

China Merchants Bank Headquarters Tower (hereafter referred to as the HQ Tower) exceeds the limits set out in current Chinese design codes for tall buildings on structural height, slenderness ratio, and horizontal and vertical structural irregularities. As a result, the performance-based seismic design (PBSD) procedure must be adopted together with the Nonlinear Response History Analysis (NRHA) method instead of the prescriptive design procedure using the linear response spectrum analysis (LRSA) method. Similar to the peer review process as an integral part of the PBSD procedure in the United States, PBSD of code-exceeding tall buildings in China must pass a vigorous and rigorous expert panel review process in order to gain statutory construction permits. Furthermore, NRHA of supertall buildings exceeding 300 m in structural height subjected to Maximum Considered Earthquake (MCE) shaking must be performed by two independent analysis teams employing two independent computer analysis software packages and two different structural mechanics models for the purpose of validation. This paper presents the PBSD procedure, seismic performance objectives and results of NRHA and seismic performance evaluation of the HQ Tower achieved by the Foster + Partners structural design team using Perform3D in comparison with those achieved by an independent team from Shenzhen Lipeng Engineering Research & Structural Design employing Midas Gen.

2. Exceptions to Building Code Provisions

The 2015 edition of the Ministry of Housing and Urban-Rural Development document (MOHURD, 2015) defines the scope of code-exceeding tall buildings in China. Tall buildings (1) using alternative structural systems not listed in Chinese design codes JGJ 3-2010 (MOHURD, 2010) and JGJ 99-2015 (MOHURD, 2015), or (2) exceeding the height limits prescribed in these two standards, or (3) having three or more horizontal and/or vertical structural irregularities irrespective of height, or (4) having one extreme structural irregularity plus another extreme or non-extreme structural irregularity, or (5) having complex configurations such as two or more towers connected by a common podium or a link bridge, or (6) having high level transfers or using slab transfers of columns, are classified as code-exceeding buildings for which the PBSD procedure must be adopted as an alternative route to the prescriptive procedure.

The height of the HQ Tower significantly exceeds the 190 m limit specified in JGJ 3-2010 (MOHURD, 2010) on reinforced concrete core - composite perimeter moment-resisting frame systems located in a moderate seismic zone in China (Chinese seismic zone 7) such as Shenzhen.

In addition, the HQ Tower exhibits five types of horizontal and vertical structural irregularities. However, neither extreme structural irregularities nor complex configurations exist in the structural configuration of the HQ Tower. The five types of horizontal and vertical structural irregularities present in the HQ Tower are as follows:

• Torsional irregularity: The maximum storey drift/displacement, computed including accidental torsion, at one end of the structure transverse to an axis is 1.35 times the average of the storey drifts/displacements at the two ends of the structure. This is caused by the side core plan configuration.

• Diaphragm discontinuity irregularity: Each of the sky lobby levels has a cut-out area exceeding 50% of the gross floor area.

• Stiffness-soft story irregularity: The lateral stiffness in the storeys below the refuge levels where outrigger and belt trusses are located is less than 90% of that in the refuge storeys.

• Vertical geometric irregularity: The horizontal dimensions of the lateral force-resisting system of storeys above the two setback levels are reduced by more than 25% of those below the two setback levels.

• In-plane discontinuity in vertical lateral force-resisting element irregularity: Four perimeter columns above the refuge levels 63 and 71 are discontinued and are transferred by primary and secondary transfer trusses in the refuge storeys.

3. PBSD Procedure, Performance Objectives and Analysis Methods

3.1. Building Performance Objectives and Analysis Methods

The two-step PBSD procedure for tall buildings in China as outlined in JGJ 3-2010 (MOHURD, 2010) is similar to that recommended in the PEER TBI Guidelines (PEER, 2017).

In the first, LRSA and linear response history analysis (LRHA) are performed to evaluate effects induced by the Service Level Earthquake (SLE) shaking having a return period of 50 years. The building seismic performance objective subjected to SLE shaking is no structural damage and minimising non-structural damage by Load and Resistance Factor Design (LRFD) and limiting storey drifts.

In the second, NRHA is performed to evaluate deformation and force demands induced by MCE shaking having a return period of approximately 2,500 years and to verify performances of deformation-controlled and force-controlled members/actions to achieve the Life Safety (LS)/Repairable damage performance objective or the Collapse Prevention (CP)/severe damage performance objective, depending on the importance classification of the tall building being designed. On aspects of nonlinear modelling and acceptance criteria on which guidance is lacking in Chinese codes, recommendations in the PEER TBI Guidelines (PEER, 2017) and ASCE 41-17 (ASCE, 2017) may be adopted and accepted by the expert review panel. In some cases, and similar to the requirement of Section 16.1.2 of ASCE 7-22 (ASCE, 2022), the performance subjected to the Design Earthquake (DE, return period of 500 years) also needs to be evaluated explicitly by a LRSA or a nonlinear static push-over analysis (NSPOA). In the case of the HQ Tower, due to the large occupant load exceeding 8,000 people, its importance classification for seismic design is raised by one grade compared with other tall buildings accommodating fewer than 8,000 people.

As a result, the building seismic performance objectives subjected to DE and MCE shaking are established and agreed upon with the expert review panel to light damage/Immediate Occupancy (IO) and repairable damage/LS, respectively. Table 1 summarises the earthquake shaking intensity levels, performance objectives and seismic analysis methods of PBSD of the HQ Tower. Figure 1 presents the 5% damped elastic response spectra associated with the three levels of earthquake shaking at the project site.

3.2. Classification of Members/Actions and Member Performance Objectives

The Chinese practice of PBSD as outlined in JGJ 3-2010 (MOHURD, 2010) classifies members in the seismic force-resisting system (SFRS) to three categories: (1) critical, (2) ordinary and (3) energy dissipating. Actions in each member are classified as either ductile/deformation-controlled or brittle/force-controlled. Acceptance limits on inelastic deformations in ductile/deformation-controlled members as recommended in ASCE 41-17 (ASCE, 2017) may be adopted pending acceptance by the expert review panel. Table 2 lists classification of members and member/action performance objectives subjected to SLE, DE and MCE shaking for PBSD of the HQ Tower based on the building performance objective listed in Table 1.

Table 1. PBSD Requirements of the HQ Tower

Level of Earthquake Shaking Intensity	Global Building Seismic Performance Objective	Seismic Analysis Method	Limits on Storey Drift Ratios
SLE	Essentially elastic, no structural damage, limiting non-structural damage	LRSA and LRHA	1/500
DE	Light structural damage/IO	LRSA or NSPOA	Not required to be verified
MCE	Repairable structural damage/LS	NRHA	1/100

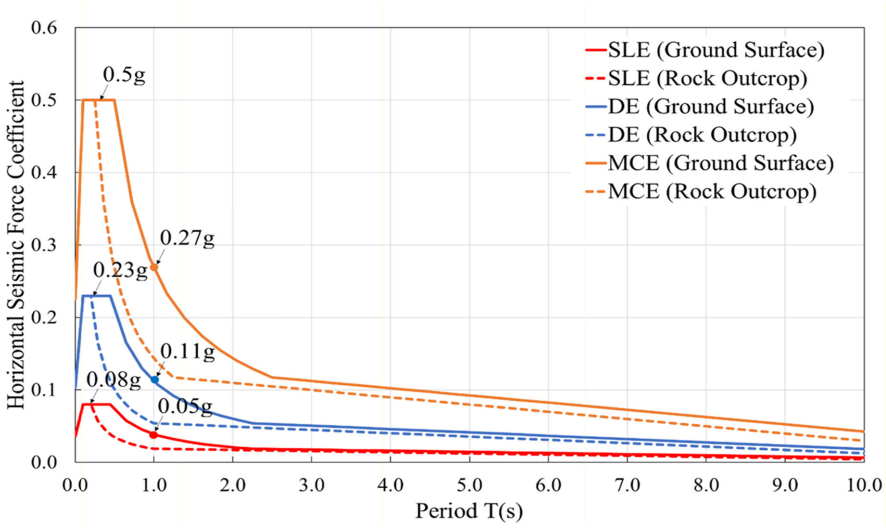


Figure 1. 5% Damped Elastic Response Spectra of SLE, DE, and MCE shaking.

4. Evaluation of Performance to SLE shaking

4.1. Analysis Model and Methods Subjected to SLE shaking and Wind Loads

Linear analysis of the HQ Tower subjected to SLE shaking and wind loads, both with a mean recurrence interval (MRI) of 50 years, is carried out using the ETABS building analysis and design computer software. The analysis model includes both the superstructure and the basement as shown in Figure 2. The foundation slab and the basement permanent retaining walls are assumed rigid, but flexibility of other structural elements in the basement including the ground slab is modelled explicitly. Walls and slabs are modelled as elastic shell elements while columns and beams are modelled using frame elements. The flexural stiffness of core wall piers and coupling beams, as well as the in-plane membrane stiffness and the out-of-plane flexural stiffness of slabs, are reduced to account for effects of concrete cracking subjected to the load combination considered. P-Δ effects are included in the analysis by considering geometric stiffness matrices of vertical structural elements. Seismic mass is determined based on the associated combination of dead and superimposed dead loads, as well as a portion of floor live load. Mass associated with the self-weight of cladding is accounted for based on the superimposed line loads applied at the perimeter of the tower. The LRSA method is employed to perform the seismic analysis to SLE

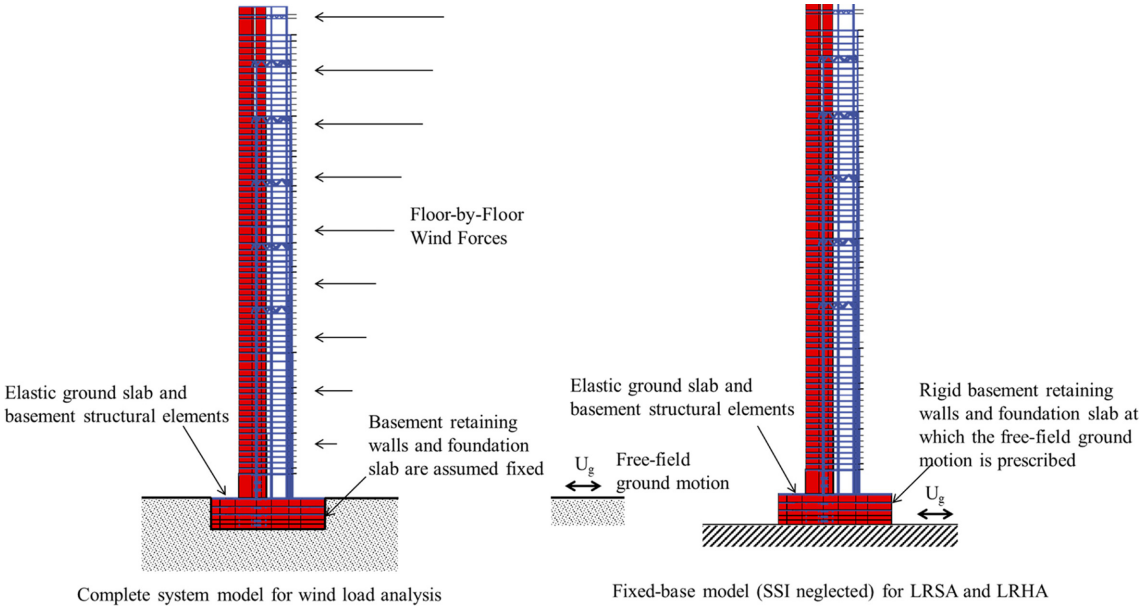


Figure 2. The Fixed-Base Linear Analysis Model of the HQ Tower with Soil-Structure Interaction Neglected.

Table 2. Member Classification and Performance Objectives

Classification of Members and Actions				Earthquake Shaking Intensity and Member Performance Objectives		
Classification	Element	Member	Action	SLE	DE	MCE
Critical	Core walls	Bottom of core wall pier plastic hinge zone and zones from one storey below to one storey above the storeys containing outrigger, transfer and belt trusses	Combined axial-flexure (ductile)	LRFD	DCR≤1.0	Plastic hinge rotation ≤ LS limits
			Shear (brittle)	LRFD	DCR≤1.0	DCR ≤1.0
	Outrigger, transfer, and belt trusses	All top and bottom chord members	Axial tension/com-pression	LRFD	DCR≤1.0	DCR ≤1.0
		Diagonal members of transfer trusses and belt trusses supporting discontinued columns	Axial tension/com-pression	LRFD	DCR≤1.0	DCR ≤1.0
	Perimeter moment frame	Discontinued columns, columns from two storeys below to two storeys above belt trusses	Combined axial-flexure (ductile)	LRFD	DCR≤1.0	Plastic hinge rotation ≤ IO limits
			Shear (brittle)	LRFD	DCR≤1.0	DCR ≤1.0
Ordinary	Core walls	Zones of core wall piers not classified as critical	Combined axial-flexure (ductile)	LRFD	Plastic hinge rotation ≤ IO limits	Plastic hinge rotation ≤ LS limits
			Shear (brittle)	LRFD	DCR ≤1.0	DCR ≤1.0
	Perimeter moment frame	Concrete-filled steel tubular (CFT) columns not classified as critical	Combined axial-flexure (ductile)	LRFD	Plastic hinge rotation ≤ IO limits	Plastic hinge rotation ≤ LS limits
			Shear (brittle)	LRFD	DCR ≤1.0	DCR ≤1.0
	Belt trusses	Diagonal concentric bracing members of belt trusses not supporting discontinued columns	Axial tension/com-pression (ductile)	LRFD	Inelastic axial elongation/ shortening ≤ IO limits	Inelastic axial elongation/ shortening ≤ LS limits
Energy Dissipating	Perimeter moment frame	Steel beams	Flexure (ductile)	LRFD	Plastic hinge rotation ≤ LS limits	Plastic hinge rotation ≤ CP limits
			Shear (brittle)	LRFD	DCR ≤1.0	DCR≤1.0
	Core walls	Reinforced concrete coupling beams	Flexure (ductile)	LRFD	Plastic hinge rotation ≤ LS limits	Plastic hinge rotation ≤ CP limits
			Shear (brittle)	LRFD	DCR ≤1.0	DCR ≤1.0
	Outrigger trusses	Diagonal Buckling-Restrained Brace (BRB) members	Axial tension/ compression(ductile)	LRFD	Axial elongation/ shortening ≤ LS limits	Inelastic axial elongation/ shortening ≤ CP limits

Note: DCR = (Force Demand) / (Strength Capacity) Ratio. For LRFD, code-prescribed load and resistance factors are applied. For performance evaluation subjected to DE and MCE shaking, all load and resistance factors are taken as unity.

shaking with the free-field ground motion applied to nodes of the foundation slab and the basement permanent retaining walls as shown in Figure 2. Accidental torsion is neglected in the LRSA in accordance with Chinese practice. The floor-by-floor wind loads determined by wind tunnel testing are applied to the floor slabs as static loads. A total of 36 wind load cases are considered, corresponding to the 36 wind directions.

4.2. Storey Shears and Overturning Moments Induced by SLE Shaking and Wind Loads

In both the East-West (E-W) and North-South (N-S) directions, the storey shears and overturning moments induced by the unfactored strength design level wind loads are approximately twice as high as those induced by SLE shaking, as illustrated in Figure 3.

Storey Drifts Induced by SLE Shaking and Wind Loads

Evaluation of factors influencing wind-indued storey drifts are presented in the companion paper (Duan, Hou and Liu, 2024). The same methodology is adopted to evaluated storey drifts induced by SLE shaking. As shown in Figure 4, the storey drift ratios induced by SLE shaking are substantially lower than those induced by the unfactored wind loads and the limit of 1/500 listed in Table 1 for meeting the global performance objective subjected to SLE shaking.

4.4. LRFD of Members

LRFD of structural members is primarily governed by wind loads rather than SLE shaking. The fibre cross section model is employed to compute the three-dimensional axial force-biaxial bending (P-M-M) strength capacity surfaces of core wall flexural piers and CFT columns.

The P-M-M strength capacity surfaces are determined based on uniaxial stress-strain curves of concrete, structural steel and reinforcement. These calculations consider the ultimate compressive strain capacity of approximate 0.0035 at the extreme compressive fibre of unconfined concrete and design strength values which incorporate partial material safety factors. The contribution of concrete tensile strength is neglected. Figures 5 and 6 illustrate cross sections of a typical core wall flexural pier and a typical CFT column, respectively, together with their three-dimensional P-M-M design strength capacity surfaces and their P-M-M force demands corresponding to the various load combinations and represented by points inside the three-dimensional P-M-M spaces. P-M-M force demands of flexure piers and shear force demands of shear piers are computed by section-cuts through the shell element mesh and stress integration. Force demand points within the strength capacity surfaces imply DCRs lower than 1.0.

The capacity design principle is implemented in the strength design of structural members and connections, such as strong shear-weak bending and strong connections-weak members, in order to ensure ductile energy dissipation mechanisms when subjected to DE and MCE shaking.

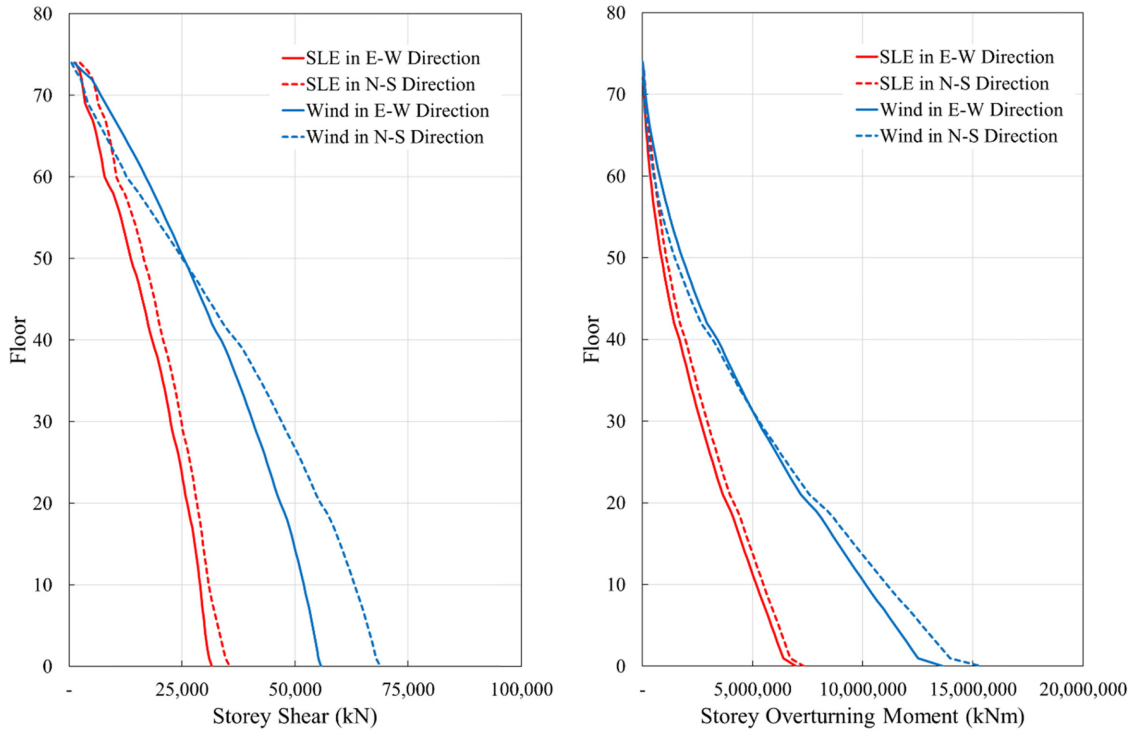


Figure 3. Storey Shears and Overturning Moments induced by SLE shaking and Wind Loads.

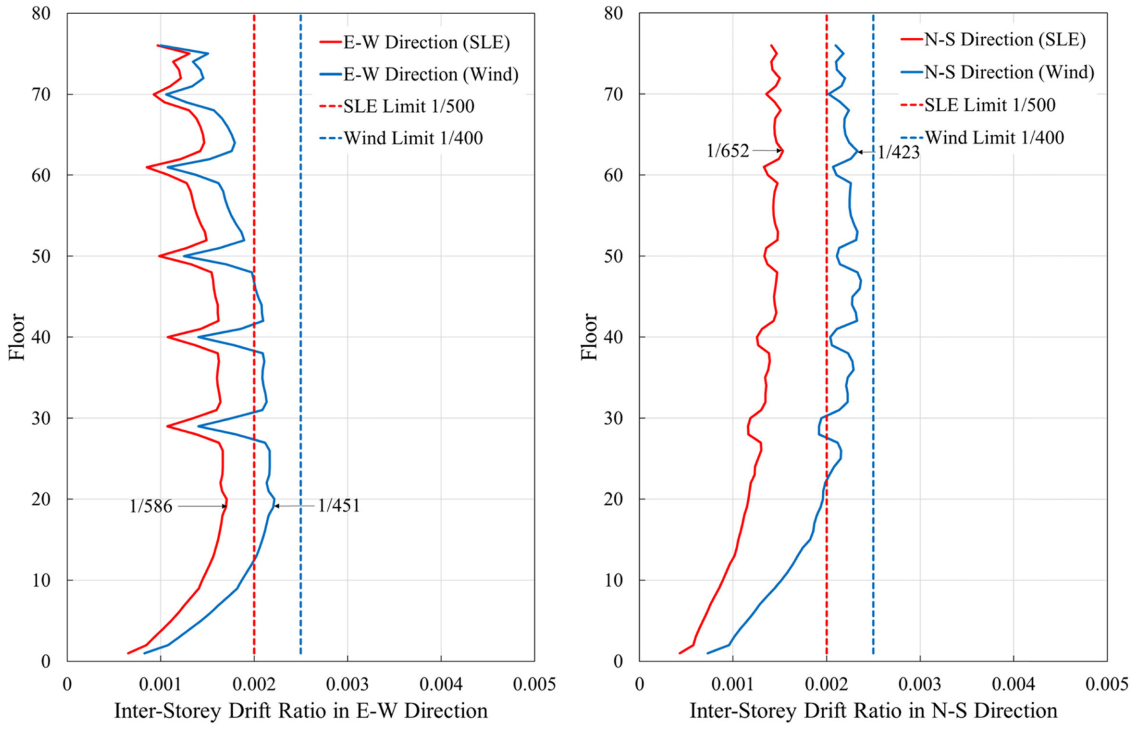


Figure 4. Inter-Storey Drifts Ratio by SLE shaking and Wind Loads.

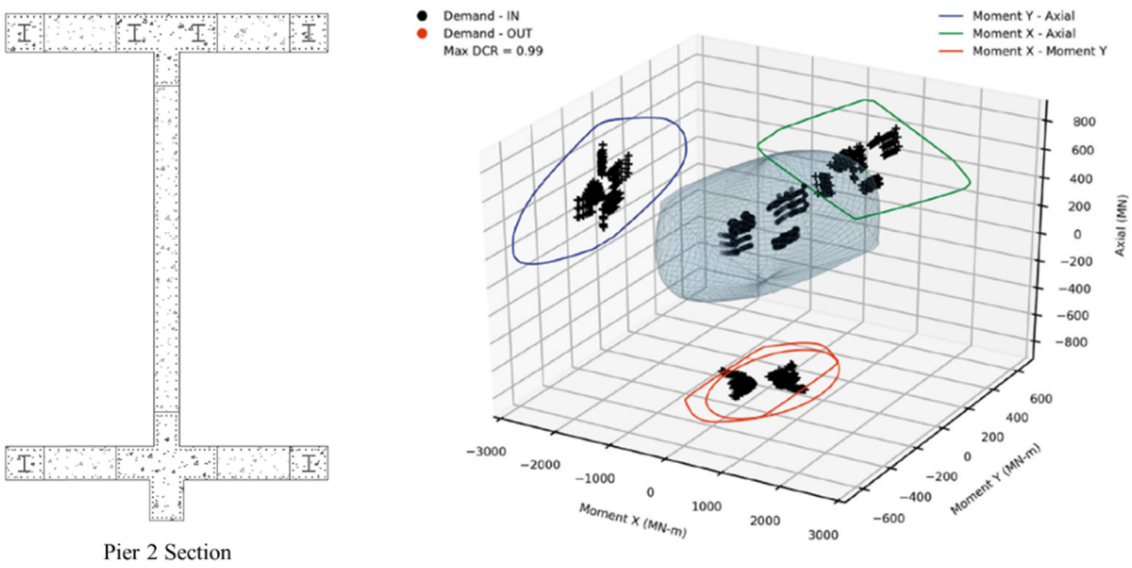


Figure 5. Cross Section, P-M-M Design Strength Capacity Surface and Force Demands of Core wall Pier 2 (Horizontal Reinforcement Not Shown).

5. Evaluation of Performance to DE and MCE Shaking

5.1. Selection, Magnitude Scaling and Spectrum Matching of MCE Ground Motion Time Histories

A suite of seven sets of tri-axial ground motion time histories is selected and magnitude scaled as MCE ground motion time histories for NRHA of the HQ Tower. For each set, the same magnitude scaling factor is applied to all three components. In accordance with current Chinese practice of PBSD of tall buildings, two horizontal pairs are further spectrum matched to the 5% damped MCE target response spectrum. All vertical components are magnitude scaled only without spectrum matching. Explicit

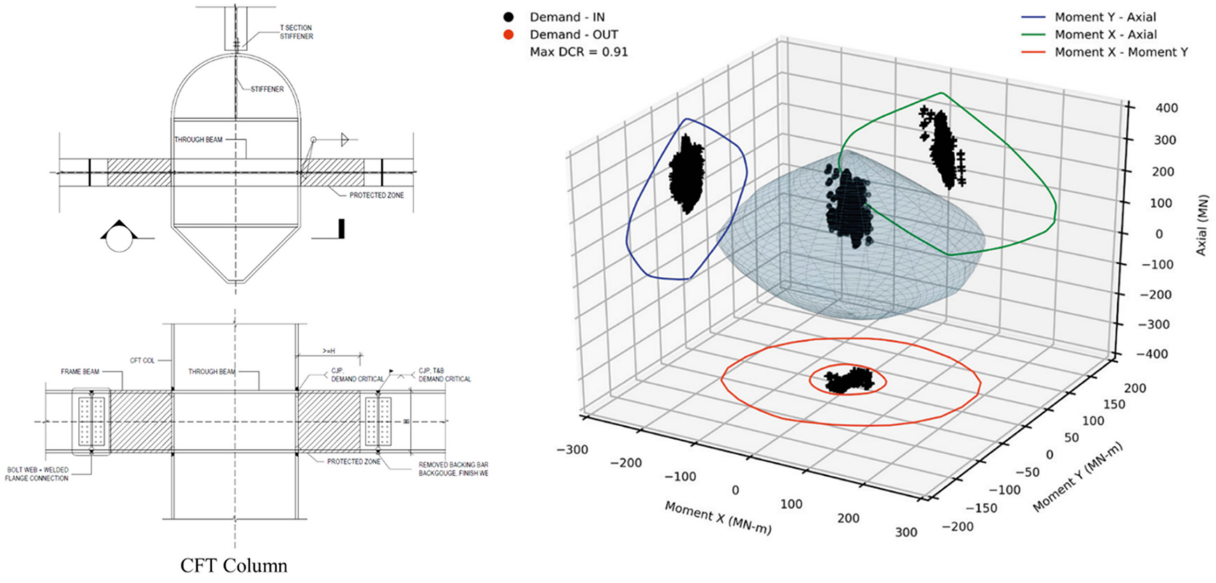


Figure 6. Cross Section, P-M-M Design Strength Capacity Surface and Forces Demands of a Typical CFT Column.

simulation of vertical earthquake response is performed due to the discontinuities in some of the perimeter moment frame columns supported by long-span transfer trusses at the two setback levels.

The original records of the seven sets of earthquake ground motion time histories are selected from the PEER strong motion databases using its searching engine based on the order of best matching the MCE target response spectrum after magnitude scaling. Figure 7 lists the Record Series Numbers (RSNs) of the selected records and presents the 5% damped response spectra of the seven stronger horizontal components after magnitude scaling of all seven sets and spectrum matching of the two horizontal pairs of RSN-40 and RSN-54. Also presented in Figure 7 are the mean spectrum of these seven achieved spectra, along with the target MCE response spectrum for the purpose of comparison.

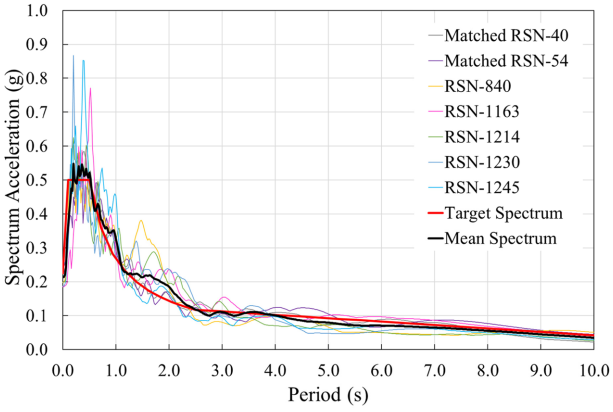


Figure 7. Response Spectra of the Stronger Horizontal Component of Selected Ground Motion Records after Magnitude Scaling and Spectrum Matching.

5.2. Perform3D and Midas Gen Nonlinear Structural Models for NRHA and NSPOA

5.2.1. Boundary Conditions

For NRHA and NSPOA, both the Perform3D and the Midas Gen nonlinear structural analysis models are further simplified from that shown in Figure 2 by deleting the basement and assuming that the superstructure is fixed at the ground slab level at which the MCE free-field ground motion time histories are applied as the prescribed boundary motion.

5.2.2. Material Strength Values

The expected strength values of structural materials are adopted for determination of stiffness of all reinforced concrete and composite structural members as well as strength of all deformation-controlled actions/members. When evaluating performance of force-controlled actions/members, the design strength values, which incorporate partial material safety factors, are adopted for evaluation of strength capacities of these actions/members.

5.2.3. Equivalent Viscous Damping

Equivalent viscous damping is assumed to be 2.5% of critical as recommended in PEER TBI Guidelines (PEER, 2017). In the Perform3D model, the equivalent viscous damping is implemented by a combination of modal damping and Rayleigh damping matrices, while in the Midas Gen model this is implemented by the Rayleigh damping matrix.

5.2.4. Modelling of CFT Columns

In both nonlinear models, CFT columns are modelled as frame elements and the lumped plasticity model is employed to model their material nonlinear behaviour. Their initial elastic flexural stiffness is reduced from

gross stiffness by a stiffness modification factor of 0.7 to consider cracking of concrete. P-M-M lumped plastic hinges are assigned to both ends of CFT columns. The initial P-M-M yielding surfaces are computed using the fibre section analysis method based on the expected material strength values, considering P-M-M action as deformation-controlled. The modelling parameters of P-M-M plastic hinges in both computer software packages are calibrated to closely match the surfaces computed using the fibre section analysis method.

5.2.5. Modelling of Core Wall Coupling Beams and Perimeter Moment Frame Steel Beams

In both Perform3D and Midas Gen models, reinforced concrete coupling beams and steel beams are modelled as frame elements with the material nonlinear behaviour modelled by the lumped plasticity model. Lumped uniaxial flexural plastic hinges about their major axis are assigned to both ends of beams. The initial elastic flexural stiffness of coupling beams is reduced from the gross stiffness by a stiffness modification factor between 0.3 to 0.5 to account for cracking as discussed in the companion paper (Duan, Hou and Liu, 2024) in both nonlinear analysis models subjected to MCE shaking.

The span-to-depth ratio of all coupling beams ranges from 3.0 to 4.0, indicating that the reinforced concrete coupling beams are flexure-controlled. These beams are reinforced with conventional symmetric longitudinal reinforcement and closely spaced stirrups. In contrast, the composite coupling beams at refuge floors are axial-flexure-controlled and are reinforced with embedded steel sections, in addition to conventional reinforcement and stirrups. The cyclic hysteresis modelling parameters in the lumped plastic hinge model in Perform3D are calibrated based on testing results of reinforced concrete coupling beams having a span-to-depth ratio of 4.0 and a horizontal reinforcement ratio ranging between 1% to 2% (Xiao et al., 1999). Figure 8 presents cyclic hysteresis loops of two typical reinforced concrete coupling beams simulated by Perform3D. The calibrated hysteresis loops exhibit pinching, stiffness, and strength degradation consistent with the observed behaviour in tests.

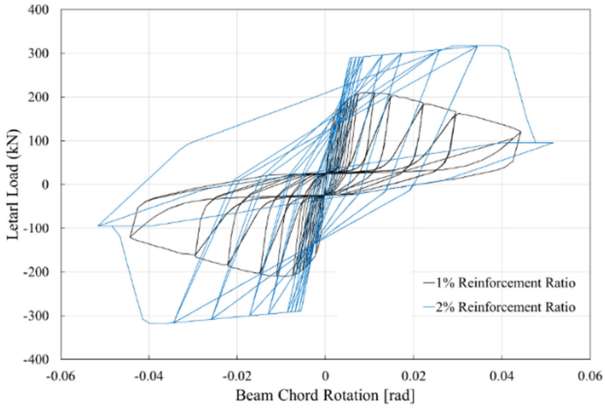


Figure 8. Perform3D Hysteresis Loops of Two Typical Coupling Beams after Calibration of Modelling Parameters.

The Takeda hysteresis model (Takeda et al., 1970) is adopted for modelling the cyclic hysteretic behaviour of reinforced concrete coupling beams in the Midas Gen model.

Plastic hinges assigned to steel beams in the perimeter moment frame exhibit a low degree of strain hardening but without any stiffness and strength degradation, nor pinching behaviour.

5.2.6. Modelling of Core Wall Piers

All core wall flexural piers are slender and are modelled by shear wall elements, which are quadrilateral shell

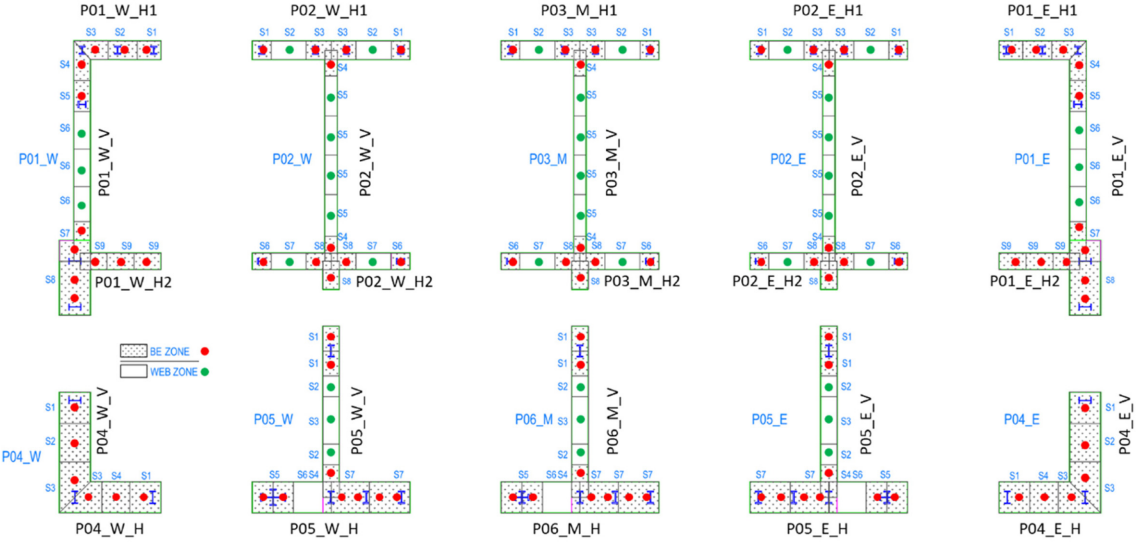


Figure 9. Core Wall Fibre Cross Section Discretisation in Perform3D.

elements with a fibre cross section formulation to model inelastic in-plane axial-bending behaviour, in the Perform3D model. Out-of-plane bending and shear as well as in-plane shear behaviour are assumed elastic. The cross sections of each and every core wall flexural piers are discretized to multiple steel, or unconfined or confined concrete fibres as shown in Figure 9. Also shown in Figure 9 are identifications of flexural piers and shear piers of the side core. Cyclic uniaxial nonlinear stress-strain relationships are assigned to the steel, unconfined and confined concrete fibres, respectively. Recommendations from recent research (Lowes et al., 2020) on nonlinear modelling of shear walls using Perform3D are adopted. The Perform3D model is capable of automatically accounting for cracking of concrete in core wall piers and the associated effects on wall stiffness. As a result, no stiffness reduction is assigned to their initial elastic stiffness.

In the Midas Gen model, core wall piers are modelled as equivalent columns using nonlinear frame elements with lumped P-M-M plastic hinges assigned at both ends of an equivalent frame element. The fibre section analysis method is utilized to compute three-dimensional P-M-M yielding surfaces for each pier and an elastic-perfectly-plastic post-yielding behaviour is assumed for the plastic hinges. Similar to the Perform3D model, the shear response of wall piers is modelled elastically. A flexural stiffness reduction factor of 0.35, as recommended by the PEER TBI guidelines (PEER, 2017) is adopted for shear walls.

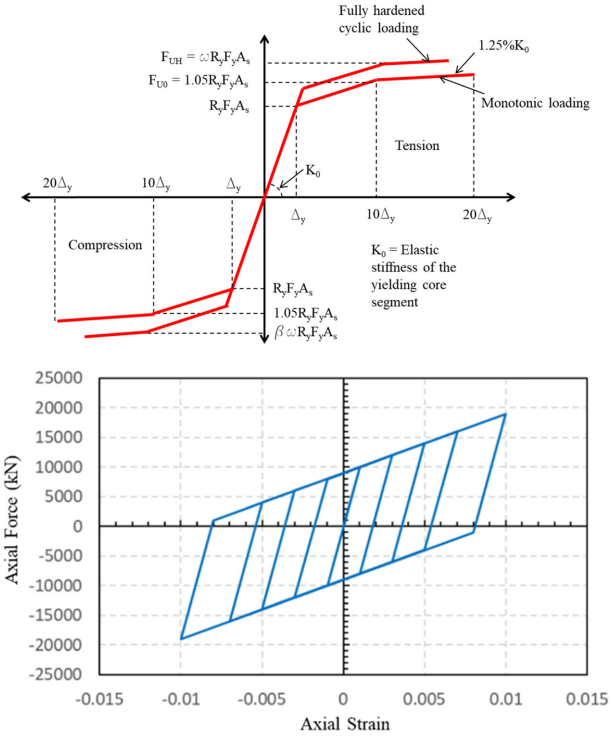


Figure 10. Axial Force-Axial Deformation Backbone Curves of the Yielding Segment in the Perform3D Model and the Hysteresis Loop of Axial Plastic Hinge in the Midas Gen Model.

5.2.7. Modelling of BRBs

Each BRB member between two joint centres is modelled by a single BRB element in the Perform3D model. The yielding region is modelled by an inelastic bar component acting in series with an elastic bar component representing the two transition regions and the two connection regions at both ends. A non-symmetric tri-linear backbone curve is adopted to model the initial elastic stiffness, yielding strength, strain hardening, post-yielding stiffness and the compression strength adjustment of the BRB component as illustrated in Figure 10.

In the Midas Gen model, each BRB member is modelled by a single elastic bar element with an axial plastic hinge assigned at the mid-point. A bi-linear backbone curve with a kinematic strain hardening rule is adopted to simulate the axial force-axial deformation relationship of the axial plastic hinge. Unloading stiffness is assumed to be equal to the initial elastic stiffness as shown also in Figure 10.

5.2.8. Modelling of Floor Diaphragm

In the Perform3D model, the floor slabs are modelled by 2D elastic shell elements with both the in-plane membrane stiffness and the out-of-plane bending stiffness reduced by a reduction factor of 0.25 to account for effects of concrete cracking and potential yielding of reinforcement in floor slabs. In the Midas Gen model, the floor slabs are assumed to be rigid in their own plane but with negligible bending stiffness.

5.3. Comparison between Key Properties of the Two Nonlinear Models

The two 3D nonlinear models are graphically shown in Figure 11. Key structural dynamics properties such as the total mass and modal periods of the first three natural vibration modes are compared in Table 3 which indicates that the match between the key structural dynamics properties is satisfactory.

Table 3. Key Structural Dynamics Properties of the Perform3D and the Midas Gen Models

Model	Total Mass (tonne)	Period of Mode 1 (sec) (Translation along the North-South Direction)	Period of Mode 2 (sec) (Translation along the East-West Direction)	Period Mode 3 (sec) (Torsion)
Perform3D	346,668	8.60	8.10	4.60
Midas Gen	342,843	8.53	7.71	4.55

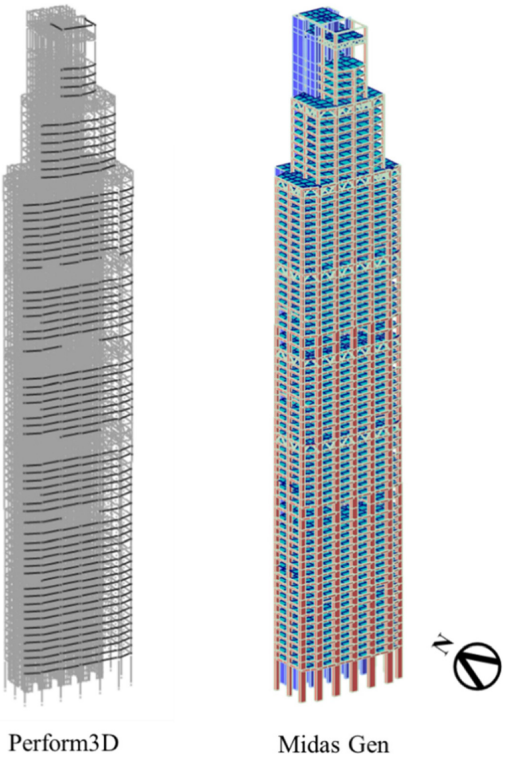
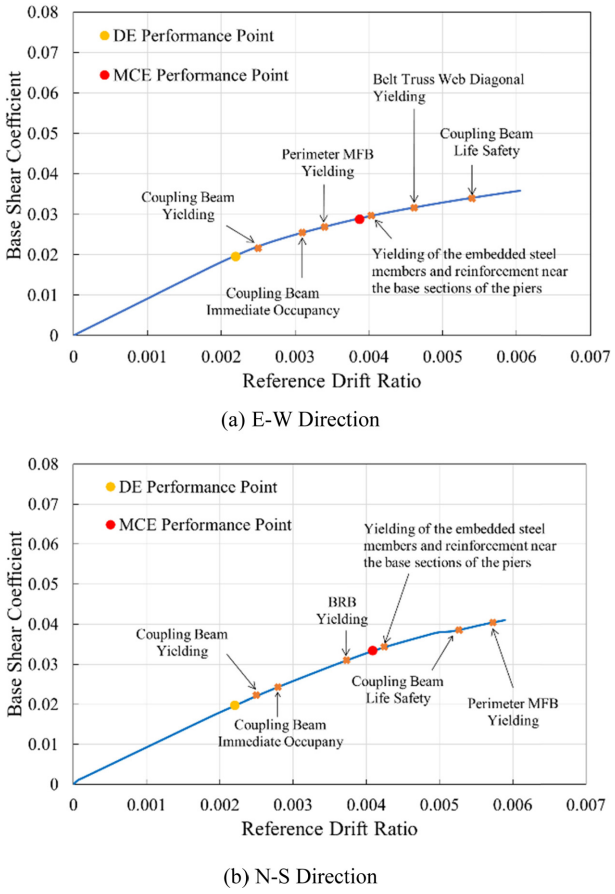


Figure 11. Perform3D and Midas Gen Nonlinear Models of the HQ Tower.



(a) E-W Direction

(b) N-S Direction

Figure 12. Capacity Curves of the Two Pushover Load Cases in Both X and Y Directions.

5.4. Evaluation of Performance to DE and MCE Shaking by NSPOA

Prior to conducting NRHA, NSPOA analysis is carried out as a first step to assess performance to DE and MCE shaking. The latter method effectively predicts the sequence of yielding and approximate inelastic deformation of deformation-controlled actions/members with high computational efficiency. This advantage allows the iterative design process, including both linear and nonlinear analysis, to progress relatively quickly, with the NRHA serving as the final step of evaluation and verification of performance to MCE shaking. The vertical distribution of the step-wise increasing lateral pushover forces along both the E-W and N-S directions follows mode shapes of the two fundamental translational modes along these two directions, respectively. The roof lateral displacements at the location of the centre of mass are the reference displacements along the E-W and N-S directions, respectively.

Figure 12 presents capacity curves of the two pushover load cases obtained from the NSPOA using Perform3D. The performance points associated with DE and MCE shaking together with key events are indicated on the capacity curves. The HQ Tower remains essentially elastic up to the event of the 1st group of coupling beams yielding and forming plastic hinges after the DE performance points. As the lateral loading increases plastic rotations in the coupling beams develop passing their acceptance limit for IO but remaining within the acceptance limit for LS when reaching the MCE performance points. The event of the 1st BRB yielding occurs after passing the DE performance point but well before reaching the MCE performance point. Yielding of steel beams in the perimeter moment frame occurs after passing the DE performance point and before reaching the MCE performance point. Plastic rotations in these beams exceed the acceptance limit for IO but remain within the limit for LS. Yielding of the embedded steel members and reinforcement near the base sections of the core wall piers occurs near but after passing the MCE performance points. No formation of P-M-M hinges in the CFT columns and no yielding or buckling of chord and web members in the belt trusses and the transfer trusses occur before the MCE performance points. The roof drift ratios which indicate the average storey drift ratios are well within the acceptance limits of 1/100 at the MCE performance point. These results demonstrate that both the global and member seismic performance of the HQ Tower to both DE and MCE shaking is satisfactory. The HQ Tower remains essentially elastic at the DE performance points and its inelastic deformations at the MCE performance points are within their respective acceptance limits. Furthermore, a desirable

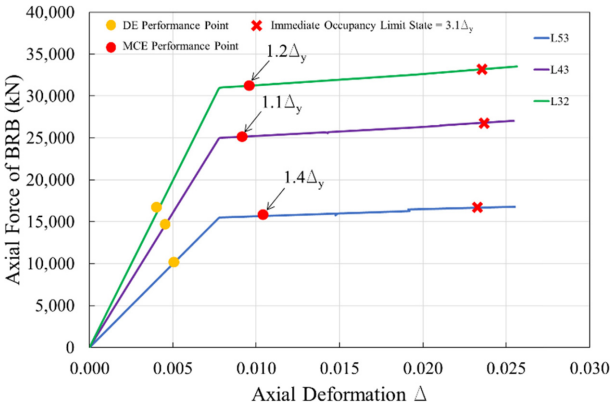


Figure 13. Force-Deformation Relationship of BRB web members in outrigger trusses on Level 32, 43, 53.

sequence of yielding is achieved meeting the seismic design intent.

Figure 13 shows the axial force-axial deformation relationship of typical BRB diagonal web members in outrigger trusses on levels 32, 43, and 53, with yielding strengths of 31.0 MN, 25.0 MN, and 15.5 MN respectively. At the MCE performance points, the axial deformation is approximately 1.1 to 1.4 times the yielding deformation and is below the acceptance limit of 3.1 times the yielding axial deformation for IO. This figure clearly demonstrates a significant benefit of using BRBs as the web members of outrigger trusses over conventional steel bracing members with the BRBs acting as structural "fuses" effectively limiting and controlling force demands in the chords, connections, CFT columns and core walls into which the outrigger trusses are anchored.

5.5. Evaluation of Performance to MCE Shaking by NRHA

5.5.1. Global performance and energy dissipation

Figure 14 presents Perform3D results of the maximum storey drift ratios induced by each of the seven sets of MCE ground motion time histories together with the average of the suite predicted by both Perform3D and Midas Gen. For the purpose of comparison, drift ratios obtained by NSPOA and the acceptance limit of 1/100 are also shown. The underprediction of effects of higher modes by the NSPOA using the fundamental mode shapes as the pattern of vertical distribution of lateral forces can be clearly observed. Close agreement between the two sets of results obtained by Perform3D and Midas Gen can also be seen. It can also be observed that the storey drift ratios induced by MCE shaking are well below the acceptance limit of 1/100, implying that the global seismic performance of the HQ Tower to MCE shaking is satisfactory.

Figure 15(a) shows a breakdown of the total external

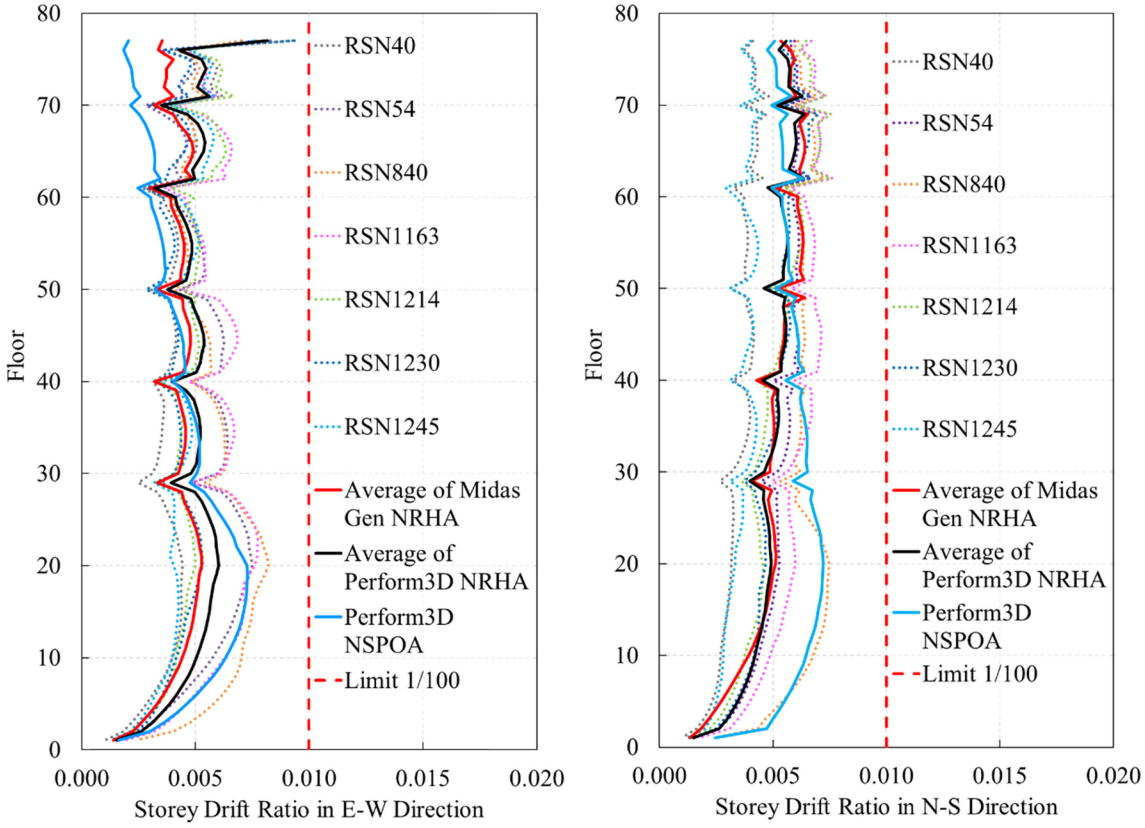
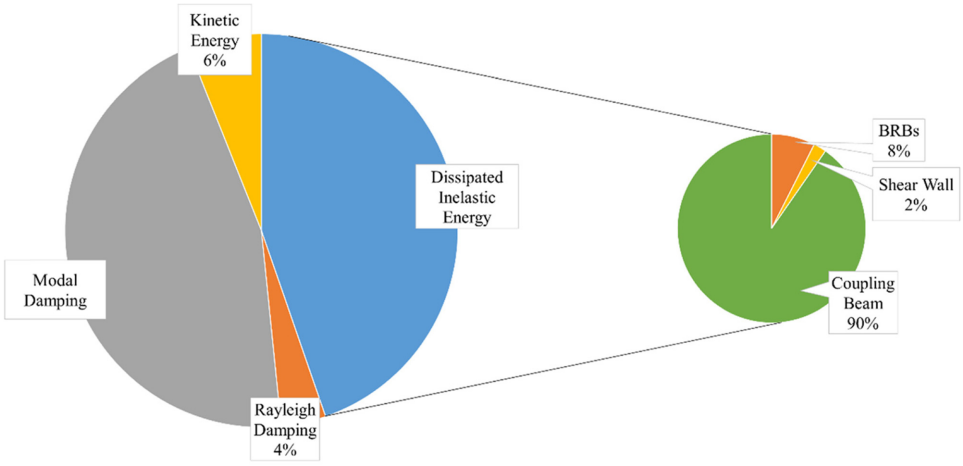


Figure 14. Storey Drift Ratios by both Perform3D and Midas Gen Results.



(a) Energy Dissipation of Complete structure (b) Energy Dissipated by Inelastic Members

Figure 15. Energy Dissipation Break-Down Diagram of Complete Structure and Dissipated Energy by Inelastic Members.

work done by a typical suite of MCE ground motion time histories to various types of energy in the structural system. At the termination of the NRHA, the structure has not yet returned to its at rest state with the kinetic energy in the lumped mass elements representing approximately 6% of the total earthquake input energy. The remaining 94% has been dissipated approximately equally by two distinct energy dissipation mechanisms – viscous damping and inelastic energy dissipated in the structural members. A further breakdown of the inelastic energy dissipated in all the structural members to various groups of members is presented in Figure 15(b). It can be observed that energy dissipated in the coupling beams accounts for 90% of the total energy dissipated in all structural members, while 8% is dissipated in BRBs and 2% is dissipated in core wall piers, respectively. These energy dissipation results demonstrate satisfactory achievement of the design intent, namely effective dissipation of a large percentage of the earthquake input energy through energy dissipating members - coupling beams and BRBs which act as structural fuse members protecting vertical gravity load carrying members – core wall piers and CFT columns.

5.5.2. Performance of Coupling Beams

Peak plastic rotations of coupling beams in selected bays obtained from Perform3D are presented in Figure 16 compared with acceptance limits for IO, LS and CP. Results of other coupling beams not shown are similar. Plastic rotations of most coupling beams are within the acceptance limit for LS. Only a few coupling beams have plastic rotations exceeding very slightly the acceptance limit for LS but considered acceptable. Those obtained from Midas Gen are lower with the maximum peak plastic rotation of all coupling beams being 0.011 radian.

5.5.3. Performance of BRBs.

Figure 17(a) demonstrates the axial cyclic force-axial

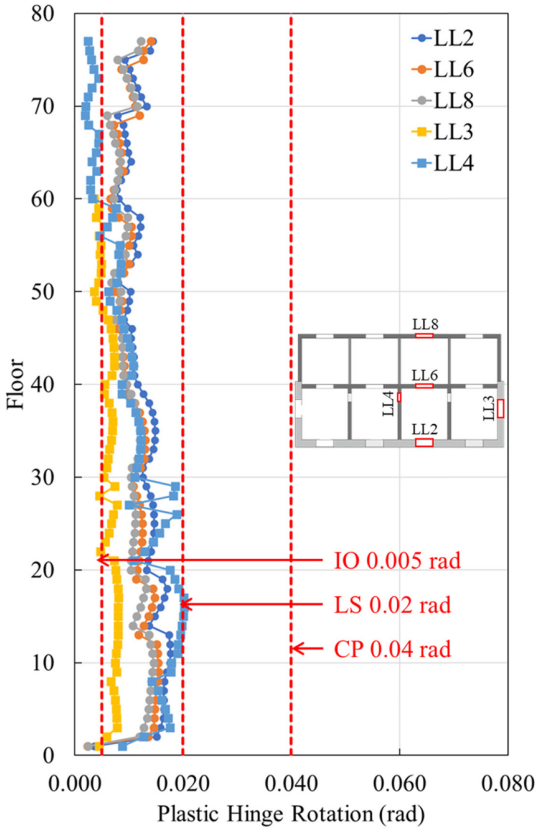
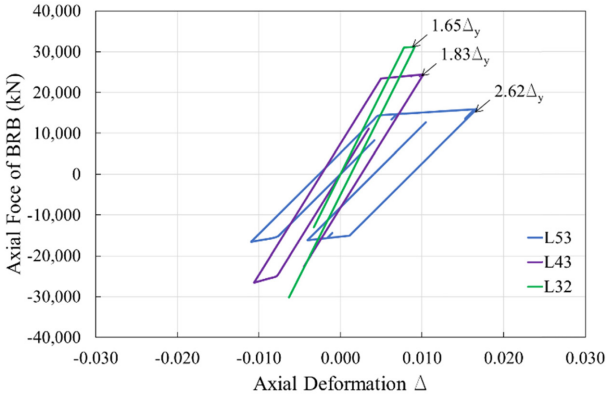
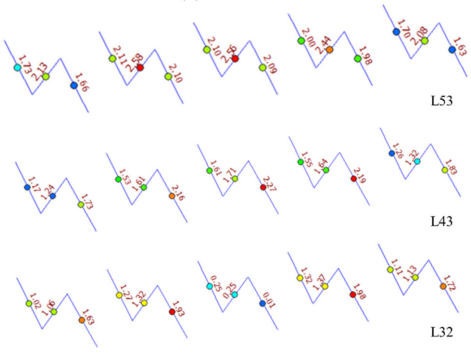


Figure 16. Coupling Beam Plastic Hinge Rotation (Average of Seven Records) by Perform3D.

deformation relationship of typical BRB diagonal web members in outrigger trusses on Levels 32, 43, and 53 obtained from Perform3D. The highest ratios between the maximum axial deformation to the yielding deformation are 1.65 on Level 32, 1.83 on Level 43 and 2.62 on Level 53, respectively. In comparison, the corresponding results from Midas Gen are 1.98 on Level 32, 2.27 on Level 43



(a) Perform3D



(b) Midas Gen

Figure 17. (a) Typical Cyclic Force-Deformation Relationships of BRBs from Perform3D, and (b) Ratios between Maximum Axial Deformation to Yielding Deformation of BRBs from Midas Gen.

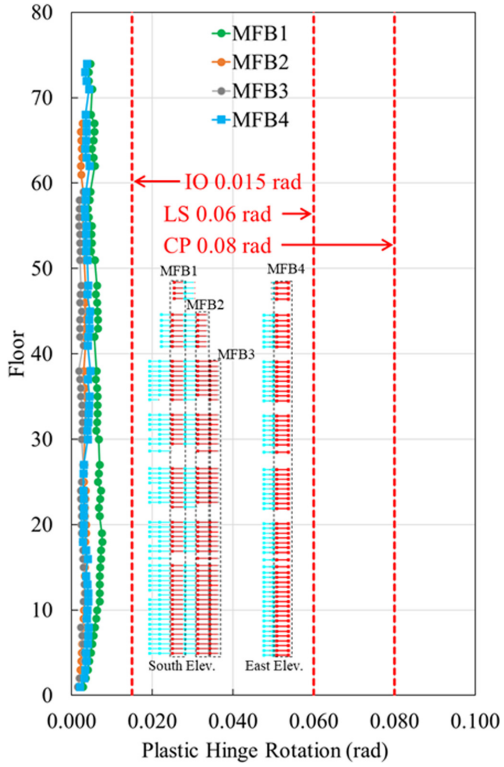


Figure 18. Plastic Rotation of Steel Beams in the Perimeter Moment Frame (Average of Seven Records) by Perform3D.

and 2.58 on Level 53, respectively as shown in Figure 17(b). The agreement between the two sets of results is satisfactory. Axial deformations of all BRBs are lower than the acceptance limit of 3.1 times their yielding deformation for IO.

5.5.4. Performance of Steel Beams in the Perimeter Moment Frame

All built-up steel beams are classified as highly ductile members, and their connections to the CFT columns are designed as beam-continuous with through-diaphragms as illustrated in Figure 6. These design measures achieve a high beam plastic rotation capacity at the beam-column connections. Acceptance limits on beam plastic rotations are estimated as 0.015 radians for IO, 0.06 radians for LS and 0.08 radians for CP, respectively, based on recommendations of ASCE 41-17 (ASCE, 2017). As shown in Figure 18, plastic rotations of the steel beams are low and well within the acceptance limit for IO. The highest steel beam plastic rotation reached is approximately 0.01 radians occurring in the lower tiers of the south elevation.

5.5.5. Core Wall Piers

Performance of flexural piers is evaluated based on the maximum tensile and compressive strains reached in the steel and concrete fibres, respectively. That of the shear piers is assessed based on their shear force DCRs. In the Perform3D model, tensile and compressive strains of flexural piers are measured using strain gauge elements along the height and located at nine corner points of the core as shown in Figure 19. Variation of the maximum compressive strains of the nine points along the height averaged across the seven records is presented in Figure 19(a). The highest average compressive strain reached is approximately 0.0013 occurring at point 7 of the base section. At point 4 of the base section, the highest average compressive strain reached is approximately 0.0011, being slightly lower due to its proximity to the centre of the building plan layout. These results suggest that the maximum compressive strains reached at the base section of the core walls are lower than the compressive strain of around 0.002 at the peak compressive stress and are approximately 1/3 of the ultimate strain capacity of approximately 0.0035 of unconfined concrete. Variation of the maximum tensile strains of the same nine points along the height of the core is presented in Figure 19(b). The highest averaged tensile strains occur at points 7, 8 and 9 of the bottom tier of the side core, with the tensile strain at the corner point 7 being the largest at 0.0024. The maximum tensile strains reached at points 1 to 6 are much lower.

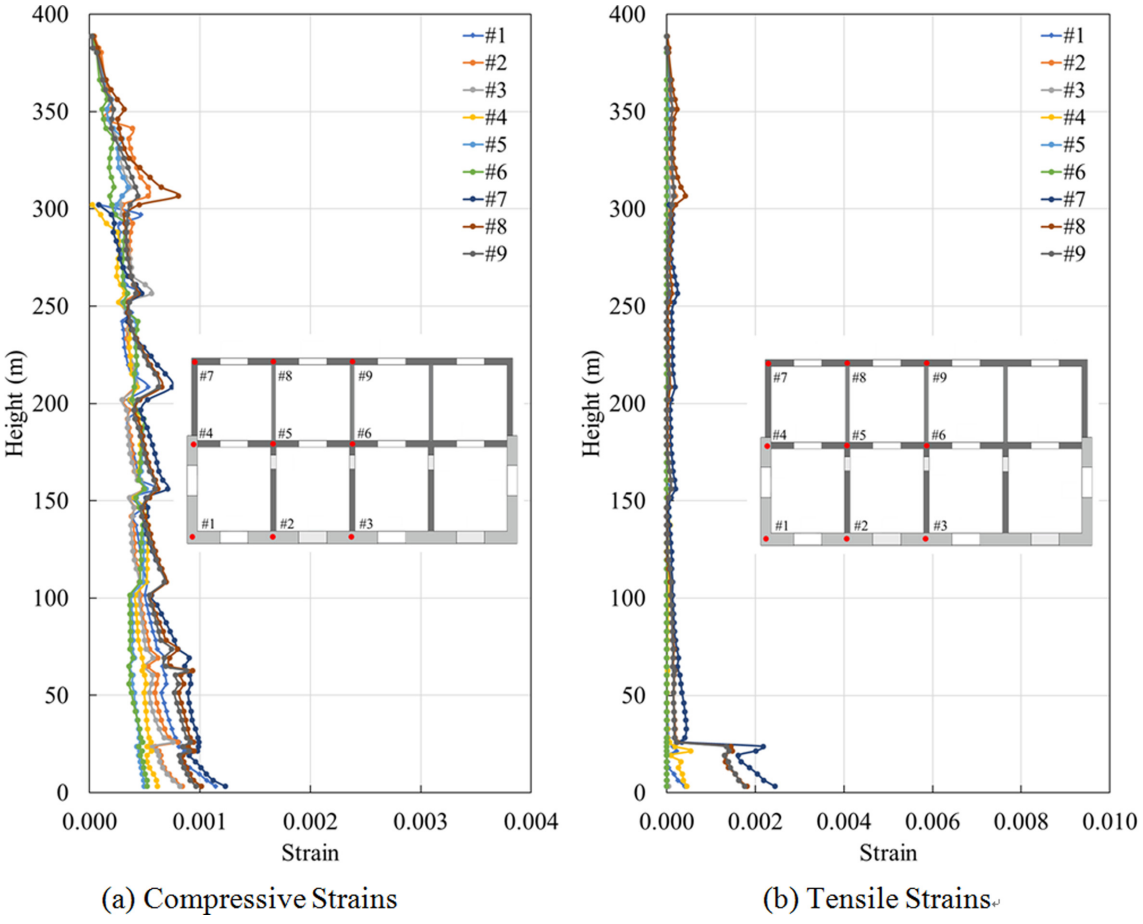


Figure 19. Wall Strains (Average of Seven Records for Sample Walls) by Perform3D.

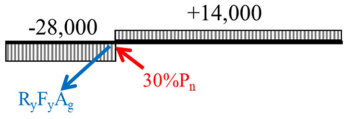
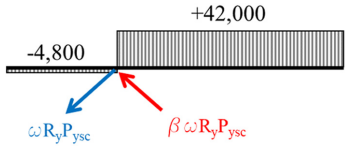
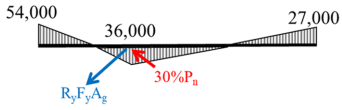
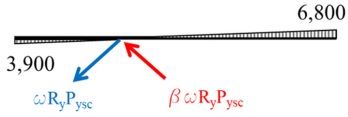
The above results indicate that the tensile strains in the reinforcement bars in the bottom tier of the flexural piers near the north façade reach or slightly exceed the yielding strain when subjected to MCE shaking. However, neither plastic hinges form nor plastic rotations develop in the plastic hinge regions near the base sections of the flexural piers, since the full plastic moment capacities of the flexural piers have not yet been reached. Results obtained from Midas Gen reveals that formation of P-M-M hinges does not occur in any of the flexural piers, confirming Perform3D results. On the basis of these observations, it appears that confinement of the boundary zones for high ductility, although implemented in the design of this supertall building in accordance with current Chinese practice, may not be necessary and detailing of the boundary zones may be simplified for ease of construction.

The axial force and shear force time histories of each and every shear pier induced by all seven MCE ground motion time histories are obtained by section-cuts in the Perform3D model and equivalent columns in the Midas Gen model. For each record and each shear pier, the maximum axial tensile force and its corresponding shear force as well as the maximum shear force and its corresponding axial force are selected as critical events at which the nominal shear stress of shear piers are evaluated. For each shear pier, the envelop value of its nominal shear stress out of all seven records are identified and are required to be lower than 4.13 N/mm^2 (equal to $0.15f_c$, the limiting value of nominal shear stress as specified by JGJ 3-2010 (MOHURD, 2010), where f_c is the concrete design compressive strength value which incorporates a partial material safety factor). Table 4

Table 4. Nominal Shear Stress of Shear Piers at the Bottom Tiers by NRHA

Shear Pier Label	Shear Pier Length (mm)	Shear Pier Thickness (mm)	Nominal Shear Stress (N/mm^2)	
			Perform3D	Midas Gen
P01_W_ H1	4,750	1,000	0.56	0.43
P02_W_ H1	7,500	1,000	0.94	0.90
P03_M_ H1	7,500	1,000	1.00	0.88

Table 5. Comparison of Chord Forces and Sections: Conventional Steel Concentric Braces vs. BRBs

Chord Member / Options	Conventional Steel Concentric Braces	BRBs
Size	Section area: 496,000 mm^2 Section depth: 1,200 mm	Area of the steel core: 241,600 mm^2 Section depth: 800 mm
Axial (kN) (+ implies tension and - implies compression		
Moment (kNm)		

shows envelop values of nominal shear stress of the presentative shear piers at the bottom tiers calculated by both Perform3D and Midas Gen. The envelop shear stresses in the shear piers are low compared with the limiting value of 4.13 N/mm^2.

5.5.6. CFT Columns

No plastic hinge formation is detected in any CFT columns in the seven nonlinear response time histories of Perform3D, nor of Midas Gen.

5.5.7. Other Steel Members

The DCRs of other steel components are assessed at every time step in each and every nonlinear response time history obtained from both Perform3D and Midas Gen. All DCRs of other steel members are lower than unity, suggesting that all other steel members remain essentially elastic without yielding.

6. Benefits of BRBs

Adopting BRBs as diagonal web members of the outrigger trusses benefits the integrated design of architectural, structural and building services engineering of the HQ Tower on several fronts:

- Improving performance subjected to MCE shaking – as described in Section 5, a relatively small number of BRBs significantly enhance energy dissipation along the north-south direction, supplementing energy dissipated by the coupling beams in the five bays of the coupled core walls along this direction. BRBs yield in both tension and compression and are therefore superior as energy dissipating members than conventional steel concentric braces which buckle in compression.
- Acting as structural fuses – ductile yielding of BRBs limits forces delivered to the CFT columns thereby benefiting the performance CFT columns by preventing axial yielding and crushing of the CFT columns.
- Minimising unbalanced forced delivered to the chords of outrigger trusses – BRBs yield in both tension and compression resulting in negligible unbalanced forces delivered to the chords of outrigger trusses thereby minimising the depth of the sections of the chords. This benefit can be clearly demonstrated by considering conventional steel concentric braces as alternatives to BRBs. Similar to the US practice of designing concentrically braced frames (AISC, 2022), the Chinese standard JGJ 99-2015 (MOHURD, 2015) also requires that the post-buckling strength of conventional steel concentric braces shall be taken as 30% of their initial buckling strength and that both chords shall be continuous. Table 5 summarises the unbalanced forces delivered to the chords, axial forces and bending moments at a typical brace-to-top chord joint for both alternative designs.

Results presented in Table 5 clearly indicate another benefit of adopting BRBs over conventional steel concentric braces – an approximately 50% reduction in steel quantity and a decrease in section depth by one-third, from an excessive 1,200 mm to a more manageable 800 mm for both the top and bottom chord. Given the architectural constraint of a floor height of 5.15 m of refuge floors, the latter is critical for achieving successful spatial coordination among integrated architectural, structural, and building services engineering designs of the refuge floors.

One structural engineering solution to alleviate the large unbalanced forces delivered to the top and bottom chords by the conventional steel concentric braces is to reconfigure the structural framing of the outrigger trusses to two-storey X- or zipper-braced frames (AISC, 2022). However, this structural solution is not practical since it would require doubling the floor height of the refuge floors. Thus, had conventional steel concentric braces been adopted, it would not have been possible to achieve spatial coordination of the refuge floors given the floor height restriction and the required large dimensions of the top and bottom chords and the gusset plates. Adoption of BRBs becomes necessary.

7. Conclusions

This paper presents a recent example and the state-of-the-practice of PBSD of code-exceeding supertall buildings exceeding 300 m in China – the performance-based seismic design of the China Merchants Bank Headquarter Tower. In addition to an expert panel review process, nonlinear response history analysis of code-exceeding tall buildings taller than 300 m in height is required to be carried out by two independent analysis teams using two different structural mechanics models and two independent analysis software. This paper clearly demonstrates benefits of the current Chinese practice of PBSD of tall and supertall buildings in terms of validation of NRHA results as well as added confidence.

This paper also clearly demonstrates benefits of energy dissipating outriggers using BRBs as diagonal web members. When subjected to MCE shaking, the BRBs not only dissipate a significant amount of energy thereby significantly improving the energy dissipation capacity of the global structure but also act as structural fuses limiting and reducing the force demands in the chord members of the outrigger trusses and the joints along the load paths compared with conventional concentric steel diagonal web members. After Beijing Yintai Centre (Li et al., 2007), One Ricon Hill in San Francisco (Klemencic et al., 2008), and Wilshire Grand in Los Angeles (Joseph, L. M., et al., 2016), China Merchants Bank Headquarters Tower is currently the world's tallest building with energy dissipating outrigger trusses using BRBs as web diagonal members.

Finally, this paper demonstrates a potential opportunity for simplifying detailing of the boundary elements in shear walls which are often congested with confinement reinforcement bars due to the prescriptive code requirement for confinement of concrete to achieve high ductility capacity. In regions of high typhoon but moderate seismicity, such as Shenzhen and Hong Kong, wind loads on tall and supertall building are often higher than those induced by DE shaking. Results achieved in this paper shows that when subjected to MCE shaking, the compressive strains of concrete in the boundary elements of the base sections of core walls are relatively low. As a result, it appears that in such cases confinement of the boundary zones for high ductility, although implemented in the design of this supertall building, may not be necessary and detailing of the boundary zones may be simplified for ease of construction. Further research is needed and is recommended on this subject.

References

American Institute of Steel Construction (2022). AISC 341-22 Seismic provisions for structural steel buildings, AISC, Chicago, IL.

American Society of Civil Engineers (2017). ASCE Standard 7-16 Minimum design loads and associated criteria for buildings and other structures, ASCE, Reston, VA.

American Society of Civil Engineers (2017). ASCE Standard 41-17 Seismic evaluation and retrofit of existing buildings, ASCE, Reston, VA.

Duan, X., Hou, Y., and Liu, M. (2024). "Structural Design of China Merchants Bank Headquarters Tower: Part 1-System and Design." International Journal of High-Rise Buildings, 13(4), 333-348.

Joseph, L. M., Gulec, C. K., and Schwaiger, J. M. (2016). "Wilshire Grand: Outrigger Designs and Details for a Highly Seismic Site." International Journal of High-Rise Buildings, 5(1), 1-12.

Klemencic, R., Hooper, J., and Johansson, O. (2008). "One Ricon Hill: Raising the Bar." Proc., Structural Congress 2008: Crossing Borders, ASCE, Reston, VA.

Li, P., Lou, Y., Zhao, G. et al. (2007). "Using Unbonded Braces in Aseismic Design for Steel Tower of Beijing Yintai Center.(in Chinese)" Building Structure, 37(11), 5-7.

Lowes, L., Lehman, D., and Baker, C. (2020). "SP-339-11: Recommendations for Modeling the Nonlinear Response of Flexural Reinforced Concrete Walls Using Perform." American Concrete Institute Special Publication-339: Performance-Based Seismic Design of Concrete Buildings: State of the Practice, ACI, Farmington Hills, MI.

Ministry of Housing and Urban-Rural Development (2010). JGJ 3-2010 Technical specification for concrete structures of tall building, MOHURD, Beijing.

Ministry of Housing and Urban-Rural Development (2015). Key technical scope of seismic design review of code-exceeding high-rise building projects, MOHURD, Beijing.

Ministry of Housing and Urban-Rural Development (2015). JGJ 99-2015 Technical specification for steel structure of tall building, MOHURD, Beijing.

Pacific Earthquake Engineering Research Center (2017). Tall building initiative guidelines for performance-based seismic design of tall buildings, PEER, Berkeley, CA.

Takeda, T., Sozen M., and Nielsen N. (1970). "Reinforced Concrete Response to Simulated Earthquakes." Journal of the Structural Division, ASCE, 96(12), 2557-2573.

Xiao, Y., Esmaeily-Ghasemabadi, A., and Wu, H. (1999), "High-Strength Concrete Short Beams Subjected to Cyclic Shear." ACI Structural Journal, Vol. 96(3), 392-399.